THE JOURNAL OF PHYSICAL CHEMISTRY A

Article

pubs.acs.org/JPCA

Reduced and Exact Quantum Dynamics of the Vibrational Relaxation of a Molecular System Interacting with a Finite-Dimensional Bath

Foudhil Bouakline,[†] Franziska Lüder,[†] Rocco Martinazzo,[‡] and Peter Saalfrank*,[†]

[†]Institut für Chemie, Universität Potsdam, Karl-Liebknecht-Strasse 24-25, D-14476 Potsdam-Golm, Germany

[‡]Department of Physical Chemistry and Electrochemistry, University of Milan, V. Golgi 19, 20133 Milan, Italy

ABSTRACT: We investigate the vibrational relaxation of a Morse oscillator, nonlinearly coupled to a finite-dimensional bath of harmonic oscillators at zero temperature, using two different approaches: Reduced dynamics with the help of the Lindblad formalism of reduced density matrix theory in combination with Fermi's Golden Rule, and exact dynamics (within the chosen model) with the multiconfiguration time-dependent Hartree (MCTDH) method. Two different models have been constructed, the situation where the bath spectrum is exactly resonant with the anharmonic oscillator transition frequencies, and the case for which the subsystem is slightly off-resonant with the environment. At short times, reduced dynamics calculations describe the relaxation process qualitatively well but fail to reproduce recurrences observed with MCTDH for longer times. Lifetimes of all the vibrational levels of the Morse oscillator have been calculated, and both Lindblad and MCTDH results show the same dependence of the lifetimes on the initial vibrational state quantum number. A prediction, which should be generic for adsorbate systems is a striking, sharp increase of lifetimes of the subsystem vibrational levels close to the dissociation limit. This is contradictory with harmonic/linear extrapolation laws, which predict a monotonic decrease of the lifetime with initial vibrational quantum number.

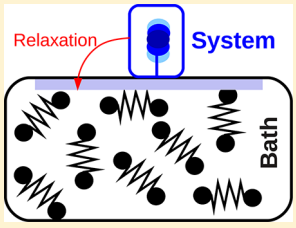

I. INTRODUCTION

Quantum dynamical processes in extended molecular systems and condensed phases are ubiquitous in nature,[1,2] and constitute a major topic of growing interest in physics and chemistry, and even in biology. Typical examples are electron or proton transfer in large biological macromolecules,[2] molecular isomerizations,[3] photochemistry in solutions and matrices,[4] and sticking of adsorbates on surfaces.[5,6]

Such dynamical problems are usually studied within the theory of open quantum systems,[7,8] for which a discrimination between primary and secondary modes is necessary. However, one cannot study the dynamics of the subsystem in isolation and completely neglect its interaction with the bath. Indeed, the inclusion of the latter is mandatory as it is required to activate the subsystem or to dissipate its excess energy.[9,10] In addition, the coupling to the bath also induces decoherence,[11,12] i.e., a loss of the phase coherence of the subsystem, a phenomenon that plays a fundamental role in quantum information[13] and quantum control of atomic and molecular processes.[14]

"Open system density matrix theory" is a so-called reduced method to treat open quantum systems,[15] where the time evolution of the reduced density matrix obeys the Liouville–von Neumann equation with an additional term that accounts for the coupling of the subsystem to the environment. This dissipative term can be derived either by a microscopic model or by using phenomenological assumptions. An example of a microscopic approach is Redfield theory,[16] which is based on projection operator techniques and perturbation theory. However, this method suffers from a lack of complete positivity, which is not consistent with a probabilistic interpretation of the reduced density matrix. To avoid this problem, Lindblad[17] and Gorini and Kossakowski[18] derived a general form of a complete positive, trace preserving dynamical semigroup Liouvillian. Both the Redfield theory and Lindblad formalism are based on many hypotheses such as the Markov approximation where memory effects are neglected, and they also fail to describe some system–bath situations like the case of an entangled initial state of the full system, or a strong coupling to the bath in the case of Redfield theory. Several ideas have emerged to generalize reduced dynamics approaches to deal with non-markovian dynamics.[19]

Another way to circumvent the problems of reduced dynamics is to treat the full system (subsystem plus bath) exactly and describe all its degrees of freedom in the same manner using an exact quantum approach. But, because of the exponential scaling of the standard quantum dynamics methods, it is impossible to deal with these large systems using current computational resources. However, tremendous progress has been recently made in this direction, especially in the development of time-dependent multiconfiguration methods such as the MCTDH (multiconfiguration time-dependent Hartree) approach.[20] This method has been successfully applied to many quantum dynamical processes in polyatomic molecules,[21] and also to adsorbate–surface problems with a large number of bath degrees of freedom.[22,23] Other variants of the method designed for true dissipative systems have also been derived, such as G-MCTDH (Gaussian MCTDH[10,25]), ML-

Special Issue: Jörn Manz Festschrift

Received: May 8, 2012
Revised: July 9, 2012
Published: July 9, 2012

   dx.doi.org/10.1021/jp304466u | J. Phys. Chem. A 2012, 116, 11118–11127

MCTDH (multilayer MCTDH[26,27]), CC-TDSCF (continuous-configuration time-dependent self-consistent field[28,29]), and LCSA (local coherent state approximation[30,31]).

In this paper, we confront exact dynamics using MCTDH with reduced dynamics in the Lindblad formalism, to examine dissipation and decoherence in a subsystem comprising a Morse oscillator that is nonlinearly coupled to a finite-dimensional bath of harmonic oscillators at zero temperature. The current study is similar to previous ones,[9,10,30] but we investigate new aspects of the problem, such as the dependence of dissipation dynamics on the discretization of the bath, in the sense that baths that are resonant and off-resonant with the subsystem are considered, and we show that the subsystem relaxation behaves differently depending on the bath discretization. We also investigate the dependence of the lifetimes of Morse vibrational states on their vibrational quantum number. The latter allows for the comparison with some extrapolation techniques,[24,39] often used in the literature to calculate dissipation rates.

The paper is organized as follows: Section II describes the subsystem−bath models under study. Section III summarizes the different theoretical approaches used in our work, namely the Lindblad reduced density matrix approach and MCTDH, as well as the different measures used to characterize the relaxation process. In section IV, we compare between reduced and exact descriptions of the dynamics for both resonant and nonresonant baths, and we also discuss the dependence of the vibrational lifetimes on the initial vibrational state of the subsystem, as well as isotopic effects. Section V concludes the paper.

II. MODEL HAMILTONIAN

The quantum calculations below consider the evolution of a "subsystem" Morse oscillator interacting with a finite-dimensional "bath" of harmonic oscillators at zero temperature. The model to be used is well documented in the literature[9,10,30] and only its main characteristics and the specific choices made in this work will be summarized here. The overall supermolecular system evolves under the Hamiltonian $\hat{H} = \hat{H}_S + \hat{H}_B + \hat{H}_{SB}$, where $\hat{H}_S$, $\hat{H}_B$, and $\hat{H}_{SB}$ describe the subsystem, the bath, and their interaction respectively, which are given by

$$\hat{H}_S = -\frac{\hbar^2}{2M}\frac{\partial^2}{\partial z^2} + D(e^{-2\alpha z} - 2e^{-\alpha z}) \tag{1}$$

$$\hat{H}_B = \sum_{b=1}^{N}\left(-\frac{\hbar^2}{2m}\frac{\partial^2}{\partial x_b^2} + \frac{m\omega_b^2}{2}x_b^2\right) \tag{2}$$

$$\hat{H}_{SB} = -\sum_{b=1}^{N} c_b f(z) x_b = -\sum_{b=1}^{N} c_b \frac{1 - e^{-\alpha z}}{\alpha} x_b \tag{3}$$

In principle, due to the subsystem−bath coupling, the Morse oscillator potential becomes distorded, and one has to add to the full Hamiltonian a counter term for renormalization.[9] However, in our work, as we are considering the weak coupling regime, this term is omitted, and the "bare" Hamiltonian above is used in all our calculations.

The numerical values of the different parameters characterizing the subsystem are chosen to be typical for a (quasi-)diatomic molecular system. In particular, a mass $M = 0.9481$ amu (the reduced mass of O−H), the depth of the potential well $D = 0.1994\ E_h$, and its parameter $\alpha = 1.189\ a_0^{-1}$ have been chosen here to roughly resemble an O−H vibration,[32] whose relaxation is to be studied. Diagonalizing $\hat{H}_S$ by using the sinc-function discrete variable representation (DVR),[34] we get 22 bound states, the fundamental frequency being $\omega_{1,0} = (E_1 - E_0)/\hbar = 3784\ cm^{-1}$ when converted to wavenumbers. The numerically obtained system eigenvalues represent well the analytical solution of the Morse oscillator, $E_v = \hbar\omega_h(v + (1/2)) - \hbar\omega_h x_e(v + (1/2))^2$, where $\omega_h = (2D\alpha^2/M)^{1/2}$ is the harmonic frequency obtained from harmonizing the Morse potential, and $x_e = \hbar\omega_h/(4D)$ is the anharmonicity constant. Here we have $\omega_h = 3951\ cm^{-1}$ and $x_e = 0.0208$.

In most studies below, the bath consisted of $N = 40$ harmonic oscillators, with masses $m = 1$ amu in all cases. The frequencies $\{\omega_b\}$ were chosen according to two different models. For a *nonresonant bath model*, the frequencies are chosen to be equidistant

$$\omega_b = b\Delta\omega \tag{4}$$

with $\Delta\omega = 153.6\ cm^{-1}$ and the cutoff frequency $\omega_N = 6145.3\ cm^{-1}$. In this case, no bath frequency matches the subsystem next-neighbor transition frequencies, but all the latter lie below the highest frequency of the bath. The cutoff frequency ω_N is higher than for a realistic condensed phase environment, at least if one thinks of the phonon bath of a solid or surface, however, we wish to consider the wide-band limit with $\omega_N > \omega_{1,0}$ in this model study.

For the *resonant bath model*, a subset of the $N = 40$ bath frequencies is chosen to match the next-neighbor transition frequencies of the subsystem. Because, for the Morse oscillator, $E_{v+1} - E_v = \hbar\omega_h - 2\hbar\omega_h x_e(1 + v)$, the corresponding bath frequencies can also be chosen equidistant in this case with $\Delta\omega = 2x_e\hbar\omega_h$. To fulfill the resonance conditions, also a shift has to be made to match the subsystem frequencies, i.e., $\omega_b = b\Delta\omega + \omega_0$ where $\Delta\omega \sim 179.5\ cm^{-1}$ and $\omega_0 \sim 14\ cm^{-1}$. This gives a cutoff frequency of $\omega_N \sim 7195\ cm^{-1}$ in this case.

Having specified the bath frequencies $\{\omega_b\}$, it is easy to derive the damping constants $\{c_b\}$ characterizing the system−bath interaction according to eq 3. In the Ohmic bath model,[9] they are given as

$$c_b = \omega_b\left(\frac{2mM\gamma}{\pi g(\omega_b)}\right)^{1/2} \tag{5}$$

where $g(\omega_b)$, the density of bath states, is chosen to be constant, i.e., $g(\omega_b) = 1/\Delta\omega$. As will be seen shortly, γ is a parameter that determines the vibrational relaxation rate of the first excited, subsystem vibrational state. Below, $\gamma^{-1} = 500$ fs will be chosen.

In the present model we use a coupling $f(z)$ that is nonlinear in the system mode. Specifically, the coupling function is $f(z) = (1 - e^{-\alpha z})/\alpha$, because we wish to describe vibrational relaxation at a surface, for which no coupling should exist at all in the limit of large values of z. Note that the coupling function becomes linear in the limit of small-amplitude motions of the subsystem relative to the surface, i.e., $f(z) \simeq z$ for very small values of z. We finally note that the fact that $\hat{H}_{SB}$ is linear in the bath coordinates and nonlinear in the subsystem coordinate allows for only one phonon transitions in the bath, and for any many-quanta transitions in the subsystem.

To avoid any confusion, we should emphasize that a finite number of harmonic oscillators can act as a "true" bath, in the thermodynamic sense, only at short times, as can be seen in the next sections. Thus, our use of the bath terminology is not in its

strict sense, i.e., a true dissipative reservoir, but as a generic term to describe a finite size environment.

III. THEORETICAL APPROACHES FOR RELAXATION DYNAMICS

In this paper, we compare reduced with "exact" dynamics as outlined above. In the first approach, we use the reduced density operator method,[15] in which we solve the Liouville−von Neumann (LvN) equation for an open system, with the help of the Lindblad formalism. In the second approach, both the subsystem and the bath degrees of freedom are treated exactly and on the same footing with a wave function method, namely the multiconfiguration time-dependent Hartree method (MCTDH).[20] As both approaches are well described in the literature, we give the reader here only a brief summary of the basic features of each method.

A. Reduced Dynamics: Lindblad Formalism and Fermi's Golden Rule. In this approach, we solve a Markovian open-system Liouville−von Neumann (LvN) equation for the time evolution of the reduced density operator $\hat{\rho} = \mathrm{tr}_B\hat{\rho}_{tot}$ (where $\hat{\rho}_{tot}$ is the total density operator and tr_B denotes a trace over bath modes).[7,8] In the Lindblad approach,[17] the Liouville−von Neumann equation is

$$\frac{\partial}{\partial t}\hat{\rho} = -\frac{\mathrm{i}}{\hbar}[\hat{H}_S,\hat{\rho}] + \sum_k \left(\hat{W}_k\hat{\rho}\hat{W}_k^\dagger - \frac{1}{2}[\hat{W}_k^\dagger W_k,\hat{\rho}]_+\right) \tag{6}$$

Here, the square brackets $[.,.]_+$ denote an anticommutator, and $\hat{W}_k$ are Lindblad operators specifying the nature and the strength of each dissipative channel (labeled by k), such as energy relaxation or pure dephasing, for which different forms were suggested.[5] In our work, we are interested in the dynamics of the vibrational energy relaxation of the subsystem, from the eigenstate $|i\rangle$ to the eigenstate $|f\rangle$ of the subsystem, i.e., $\hat{H}_S|n\rangle = E_n|n\rangle$ ($n = i, f$). In this case, the Lindblad operators $\hat{W}_k$ are conveniently chosen as

$$\hat{W}_k = \sqrt{\Gamma_{i\to f}}|f\rangle\langle i| \tag{7}$$

Now, $k = (i, f)$ is a composite index, and $\Gamma_{i\to f}$ is an environment-induced transition rate, a quantity that is computed perturbatively using Fermi's Golden Rule as described shortly. Adopting the Lindblad formalism with the dissipation operators of eq 7, the time evolution of the elements of the reduced density matrix in the subsystem state representation, is given by[5]

$$\frac{\mathrm{d}\rho_{kk}}{\mathrm{d}t} = -\rho_{kk}\sum_{i=1}^{N}\Gamma_{k\to i} + \sum_{i=1}^{N}\Gamma_{i\to k}\rho_{ii} \tag{8}$$

for the diagonal elements ("populations"), and

$$\frac{\mathrm{d}\rho_{kl}}{\mathrm{d}t} = \rho_{kl}\left[-\frac{\mathrm{i}}{\hbar}(E_k - E_l) - \frac{1}{2}\sum_{i=1}^{N}(\Gamma_{k\to i} + \Gamma_{l\to i})\right] \tag{9}$$

for the off-diagonal ($k \neq l$) elements ("coherences"). Note that in eq 9, no pure dephasing terms have been included. Within the Lindblad formalism and the chosen dissipation operators, the time evolutions of the populations and coherences of the reduced density matrix are completely decoupled. In other words, there is no population−coherence transfer, and no coherence−coherence transfer. In reality, all matrix elements of the reduced density matrix (populations and coherences) are coupled. Further, the Markov approximation may not hold in practice.

The vibrational relaxation rates of the subsystem, from an initial state $|i\rangle = |\psi_i\rangle$ to a final state $|f\rangle = |\psi_f\rangle$, have been calculated from Fermi's Golden Rule as

$$\Gamma_{i\to f} = \frac{2\pi}{\hbar}\sum_{I,F} p_I\,|\langle\psi_i\Phi_I|\hat{H}_{SB}|\psi_f\Phi_F\rangle|^2\delta(e_{i,I} - e_{f,F}) \tag{10}$$

where $I = \{i_1, i_2, ...\}$ and $F = \{f_1, f_2, ...\}$ are bath indices, $e_{i,I}$ and $e_{f,F}$ are the initial and final total energies of the full system, and p_I is the weight of the Ith bath initial state. Note that, as we are studying the case where the bath is at zero temperature, only subsystem downward transitions are possible, and only the initial state I

$$\Phi_I(x_1, ..., x_N) = \prod_{b=1}^{N}\chi_0^{(b)}(x_b) \tag{11}$$

has to be considered, with unit weight, where $\chi_v^{(b)}(x_b)$ is the harmonic oscillator wave function for the bath oscillator b in state v. Due to the linear form of $\hat{H}_{SB}$ in the bath coordinates, the only possible final states F are those describing one-phonon excited configurations of the bath, namely

$$\Phi_F(x_1,...,x_N) = \chi_1^{(k)}(x_k)\prod_{b\neq k}^{N}\chi_0^{(b)}(x_b) \equiv \Phi_k^{(1)}(x_1,...,x_N) \tag{12}$$

for a single excitation in the kth oscillator. Using the system−bath coupling $\hat{H}_{SB}$, and integrating over bath modes one gets

$$\Gamma_{i\to f} = \frac{\pi}{\hbar}\sum_{k=1}^{N}|\langle i|f(z)|f\rangle|^2\frac{{c_k}^2}{m\omega_k}\delta(\omega_{i,f} - \omega_k) \tag{13}$$

where ω_k is the harmonic frequency of the kth bath oscillator, and $\omega_{i,f} = (E_i - E_f)/\hbar$. In the Ohmic bath model, using eqs 4 and 5,

$$\Gamma_{i\to f} = \frac{2}{\hbar}|\langle i|f(z)|f\rangle|^2 M\gamma\sum_{k=1}^{N}\omega_k\delta(\omega_{i,f} - \omega_k)\Delta\omega \tag{14}$$

In the wide-band continuum limit, one can replace the discrete sum over the bath frequencies by an integral, $\sum_k g(\omega_k)\Delta\omega \to \int g(\omega)\,\mathrm{d}\omega$ and do the integral over the Dirac delta-function analytically, which gives

$$\Gamma_{i\to f} = \frac{2}{\hbar}|\langle i|f(z)|f\rangle|^2 M\gamma\omega_{i,f} \tag{15}$$

This equation further simplifies under the double-harmonic approximation, i.e., when the Morse functions are approximated as harmonic oscillator functions $\psi_v^h(z)$, and the coupling function $f(z)$ is replaced by z, to

$$\Gamma_{v\to u} = \delta_{v,u+1}\cdot v\cdot\gamma;\ v > 0 \tag{16}$$

Here, $\langle\psi_v^h|z|\psi_u^h\rangle = (v\hbar/2M\omega_{1,0})^{1/2}$ if $v = u + 1$ and 0 otherwise, has been used. Equation 16 demonstrates the equivalence $\Gamma_{1\to 0} = \gamma$ in this limit, selection rules $\Delta v = -1$, and a linear increase of the decay rate with initial quantum number, v, of the subsystem oscillator.

In practice, we do not make these approximations here but use anharmonic matrix elements $\langle i|f(z)|f\rangle$ instead, a discrete bath, and represent the delta-functions by normalized Lorentzians. That is, we use eq 14 in a form

$$\Gamma_{i\to f} = \frac{2}{\hbar}|\langle i|f(z)|f\rangle|^2 M\gamma \sum_{b=1}^{N} \omega_b \Delta\omega \frac{1}{\pi} \frac{\sigma/2}{(\sigma/2)^2 + (\omega_b - \omega_{if})^2} \quad (17)$$

We should notice that the Lorentzian broadening amounts to couple each discrete bath mode to a true dissipative bath; i.e., it introduces a secondary bath with a relaxation time proportioanl to σ^{-1}. By choosing the Lorentzian width parameter as $\sigma = \Delta\omega$, we obtain vibrational relaxation rates close to γ for the $1 \to 0$ transition, as demonstrated below.

In our calculations, we use all bound states of the Morse oscillator as a basis to represent the reduced density matrix operator. The initial state is the v_0-th excited state of the Morse oscillator, i.e.,

$$\rho_{kl} = \begin{cases} 1 & \text{if } k = l = v_0 \\ 0 & \text{otherwise} \end{cases} \quad (18)$$

The reduced density matrix propagation is done with a Newton polynomial propagator[36,37] of order 16.

B. Exact Dynamics: MCTDH. To assess the validity of the assumptions introduced in the Lindblad/Golden Rule form of the reduced density matrix for our problem, we have also performed exact quantum calculations, with the help of the multiconfiguration time-dependent Hartree (MCTDH) method.[20] In the MCTDH approach when applied to a system−bath problem, we solve a Schrödinger equation of the form

$$i\hbar\frac{\partial\Psi}{\partial t} = (\hat{H}_S + \hat{H}_B + \hat{H}_{SB})\Psi \quad (19)$$

The wave function of the whole system is expanded into a sum of Hartree products

$$\Psi(z,x_1,...,x_N,t) = \sum_{j_0=1}^{n_z}\sum_{j_1=1}^{n_1}...\sum_{j_N=1}^{n_N} A_{j_0 j_1 ... j_N}(t)\varphi_{j_0}^{(z)}(z,t) \prod_{\kappa=1}^{N}\varphi_{j_\kappa}^{(\kappa)}(x_\kappa,t) \quad (20)$$

where $A_{j_0 j1...jN}$ are time-dependent expansion coefficients and $\varphi_{j\kappa}^{(\kappa)}$ are coordinate- and time-dependent single-particle functions (SPF) for the κth degree of freedom, which are in turn defined on a time-independent primitive basis such as a discrete variable representation (DVR) grid.[33,34] Both the expansion coefficients and the SPF are variationally optimized using the Dirac-Frenkel variational principle.

The efficiency of this method over standard wavepacket methods is due to the small number of SPF required for convergence compared to the number of primitive basis functions needed to correctly describe each degree of freedom. Another important feature of MCTDH, which is exploited in our calculations, is the mode-combination technique. This allows us to combine several degrees of freedom in a generalized SPF defined on a direct product grid, and hence reducing the length of the expansion coefficient vector $A_{j0j1...jN}$. Numerical details of the MCTDH propagations are summarized in Table 1. For the solution of the MCTDH equations of motion, we use the Heidelberg MCTDH program package.[35]

The initial state of the whole system is chosen such that there is again no correlation between the subsystem and the bath,

Table 1. Grid Parameters for MCTDH Calculations[a]

mode	DVR	minimum	maximum	N_p	$n(\tilde{n})$
z (system)	sin	$-1\ a_0$	$19\ a_0$	501	15
Q_{1-7} (bath)	HO			6	4−6

[a]The DVR types are denoted "sin" for the sinc-function DVR and "HO" for the Hermite (harmonic oscillator) DVR. Minimum and maximum define the grid extentions, where known. N_p is the number of primitive grid points, and $n(\tilde{n})$ is the number of SPF for a given (combined) mode. Notice here the use of mode combination giving rise to seven combined modes of the 40 bath oscillators.

with the subsytem in state v_0, and the bath in its ground state, i.e.,

$$\Psi(z,x_1,...,x_N,t=0) = \psi_{v_0}(z)\prod_{b=1}^{N}\chi_{0_b}^{(b)}(x_b) \quad (21)$$

where $\psi_{v0}(z)$ is an eigenstate of the Morse oscillator and $\chi_{0_b}^{(b)}(x_b)$ are harmonic oscillators ground state functions. From the propagated wave function $\Psi(z,x_1,...,x_N,t)$, we can construct a reduced density matrix

$$\hat{\rho}(t) = \mathrm{tr}_B\{|\Psi(t)\rangle\langle\Psi(t)|\} \quad (22)$$

by integrating out the bath modes.

C. Analyzing Results. Once we have calculated the reduced density matrix elements at all times, with either method, it is easy to calculate the time evolution of any subsystem observable. This is done by taking the trace of the product of its corresponding operator and the reduced density matrix, i.e., $\langle\hat{O}\rangle(t) = \mathrm{tr}\{\rho(t)\hat{O}\}$. For instance, the quantities that are going to be used in the following section to quantify dissipation are the mean energy of the subsystem $\langle H_S\rangle(t)$, and the populations of the Morse oscillator vibrational states, given by $P_v(t) = \mathrm{tr}\{\hat{\rho}(t)|v\rangle\langle v|\} = \rho_{vv}$. The dissipation, described by an energy loss of the subsystem in favor of its environment, is accompanied by a decoherence of the subsystem, that is, a loss of phase information of the subsystem over time. However, in the present context, it makes no sense to talk about decoherence of the Morse oscillator, meant as the decay of the off-diagonal elements of the reduced density matrix in the subsystem state representation. This is because in the Lindblad formalism, all coherences are and remain, exactly zero in our example. In contrast, for the full MCTDH dynamics, the off-diagonal elements of the reduced density matrix can be nonzero.

Instead of decoherence, we use another measure to quantify entanglement between the subsystem and the bath, which is the purity of the reduced density matrix.[15] This quantity is defined as the trace of the square of the reduced density matrix, $\mathrm{tr}(\hat{\rho}^2)$. It is equal to unity for a pure state and to $1/M$ for a maximally incoherent mixture of M states of the subsystem.[11,12] Although the initial state of the whole system (Morse plus bath) is an uncorrelated state, the system−bath interaction entangles the total system so that the total state becomes inseparable (entangled) over time, leading thus to the decay of the purity of the reduced density matrix.

Another measure on the subsystem state is given by the von Neumann entropy

$$S = -k_B\mathrm{tr}\{\hat{\rho}\ln\hat{\rho}\} \quad (23)$$

where k_B is the Boltzmann constant. Notice that the purity defined above is a form of entropy, and it is related to what is

called "linear entropy".[8] For instance, the von Neumann entropy is equal to zero for pure states, and to (k_B ln M) for a maximally incoherent mixture of M states of the subsystem.

IV. RESULTS AND DISCUSSION

In this section, we present the main results of our calculations. We begin with the vibrational relaxation dynamics of the Morse oscillator interacting with a resonant bath, and then with a nonresonant bath, where we compare the predictions of "exact" and reduced dynamics calculations. Finally, we discuss the behavior of the lifetimes of all the vibrational states up to the dissociation limit.

A. Resonant Bath. *A.1. Lindblad Model.* The first calculations we have performed deal with vibrational relaxation of a Morse oscillator, initially in a well-defined vibrational state $|\psi_{v0}\rangle$, interacting with a resonant bath, meaning that the bath spectral density contains a subset of frequencies matching exactly all the one-quantum transition frequencies between the different eigenstates of the subsystem. This situation is ubiquitous in system−bath problems such as adsorbate−surface dynamics, where the environment is usually composed of a huge number of degrees of freedom giving rise to an almost continuous density of states. (This statement is of course only true if the subsystem transition frequency lies within the phonon band.) The calculations were performed for all the vibrations of the Morse oscillator up to the dissociation limit, using the two approaches described above.

To facilitate interpretations, we will mainly show the results for the case where the subsystem is initially in its first vibrational excited state (v_0 = 1). In Figure 1a we follow the transfer of the excess energy from the subsystem to the bath according to Lindblad calculations, where the expectation value of the energy of the Morse oscillator decays exponentially on the time scale of $\sim\gamma^{-1}$ = 500 fs and reaches a steady state after

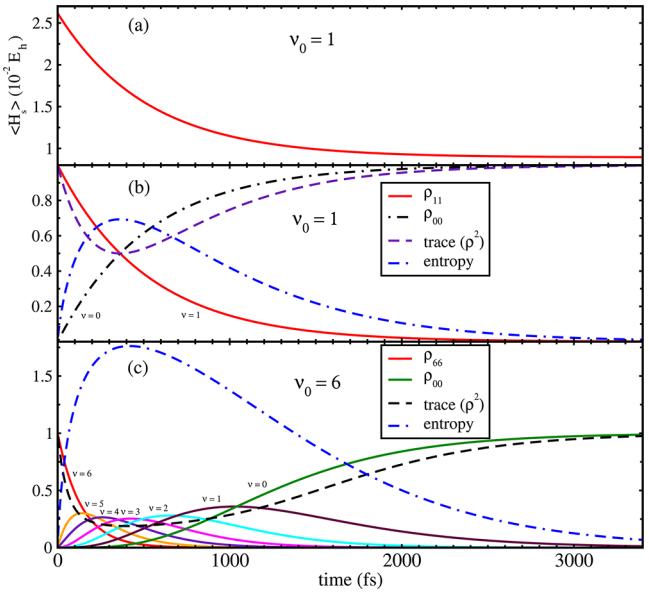

Figure 1. Vibrational relaxation of a Morse oscillator interacting with a resonant bath using reduced density matrix calculations. (a) Time evolution of the subsystem average energy with an initial vibrational state v_0 = 1. (b) Time evolution of the subsystem populations, purity and entropy (in units of k_B), where the initial vibrational state of the subsystem is v_0 = 1. (c) Same as (b) for a different initial vibrational state of the subsystem v_0 = 6.

~3000 fs, the time for which we observe a full transfer of energy from the subsystem to the bath. This is due to a population transfer in the Morse oscillator, from the initial state (v_0 = 1) to the ground state (v = 0), as shown in Figure 1b.

Figure 1b shows, in addition to populations, also the evolution of the purity of the reduced density matrix and the entropy of the subsystem. The purity of the reduced density matrix is an information measure of entanglement. At times t = 0 and $t \geq$ 3000 fs, the Morse oscillator is in a pure state, v = 1 and v = 0, respectively, which shows by the purity tr($\hat{\rho}^2$) being 1. During the time interval in between, we have a mixture of two states and the purity is smaller than 1, going through a minimum equal to 1/2 when both states are maximally mixed. This is the case after the half lifetime, $T_{1/2} \sim \ln 2\ \gamma^{-1} \sim 350$ fs. In a Lindblad two-level system at a temperature T = 0, the purity is given analytically as

$$\mathrm{tr}\,\hat{\rho}^2 = 1 - 2(e^{-t/\tau_1} - e^{-2t/\tau_1}) \tag{24}$$

where $\tau_1 \sim \gamma^{-1}$ is the vibrational lifetime of the first excited state. This behavior of the purity over time is similarly shown in the evolution of the entropy of the subsystem, but with an opposite evolution, it increases from $S(t{=}0)$ = 0, reaching a maximum at $t = T_{1/2} \sim 350$ fs, and then decreases toward S = 0 at longer times again. In the present case, the entropy is analytically given as

$$S = -k_B\left[-\frac{t}{\tau_1}e^{-t/\tau_1} + (1 - e^{-t/\tau_1})\ln(1 - e^{-t/\tau_1})\right] \tag{25}$$

giving $S = k_B$ ln 2~0.69k_B for the maximally mixed state at $t = T_{1/2}$. Note also that in the first time interval $0 < t < \tau_1$, one can observe that purity decays faster than the population of the initial state.

The general features in the evolution of the different information measures shown in Figure 1b are the same independent of the initial vibrational state of the subsystem. This is illustrated in Figure 1c where the Morse oscillator is in an initial vibrational state v_0 = 6. Again, we observe a full energy (and population) transfer at long times. However, this does not occur via the $|6\rangle \rightarrow |0\rangle$ transition, although this is (weakly) allowed, but through a cascade of transitions $|6\rangle \rightarrow |5\rangle \rightarrow |4\rangle \rightarrow |3\rangle \rightarrow |2\rangle \rightarrow |1\rangle \rightarrow |0\rangle$, where the intermediate states are populated (and then depopulated) over time. As for purity, we observe the same behavior as before, it first decays from its initial value (tr($\hat{\rho}^2$) = 1) with a higher rate than the decay of initial population, then it reaches a plateau when the state of the system gets mixed, and it finally increases to unity as the subsystem evolves toward its final pure state (v = 0). This trend is also illustrated on the same graph by the curve of the entropy of the subsystem, which increases when the system is in a mixed state and then drops toward zero when the excess energy of the Morse oscillator is completely transferred to the bath. We finally note that the decay of the initial state with v_0 = 6 proceeds on a shorter time scale than v_0 = 1. The dependence of the vibrational relaxation time on initial state v_0 will be examined below in detail.

In summary, it is obvious that the reduced density matrix does not show any size effect of the bath, but it treats it as a true infinite reservoir. The Lindblad dynamics is Markovian with an exponential population decay, and the density matrix remains diagonal if no external field or other Hamiltonian coupling mechanisms are present. The question one may ask is whether that is exactly what happens in the case of a finite bath.

dx.doi.org/10.1021/jp304466u | J. Phys. Chem. A 2012, 116, 11118−11127

A.2. MCTDH Model. To check the veracity of the previous results, we have performed exact quantum calculations where both the subsystem and the bath are treated on the same footing using the MCTDH wave function approach. Figure 2a

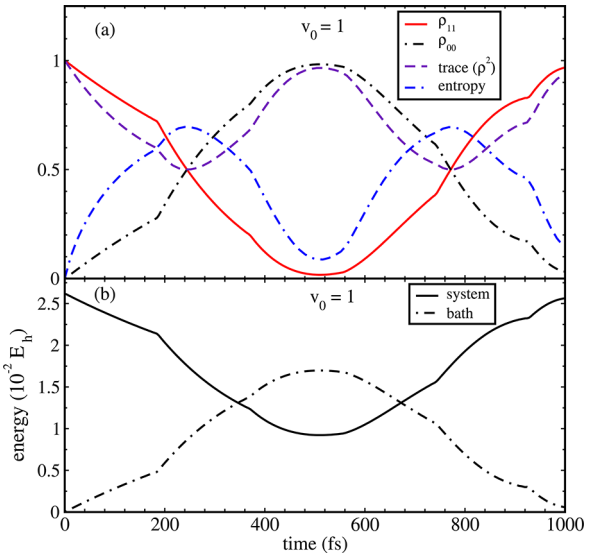

Figure 2. Vibrational relaxation of a Morse oscillator (v_0 = 1) interacting with a resonant bath using MCTDH calculations. (a) Time evolution of the subsystem populations, purity and entropy (in units of k_B). (b) Time evolution of the subsystem and the bath average energies.

shows MCTDH results for the time evolution of the same information measures as in Figure 1b, and Figure 2b shows system and bath energies, for an initial Morse oscillator state v_0 = 1, suddenly coupled to 40 bath oscillators. Up to 500 fs, we observe that the subsystem's observables behave similarly to the reduced density matrix method. The population of the initial state drops to zero while populating the vibrational ground state, the purity reaches the value 1/2 after a "half lifetime" time, which is ∼250 fs now, and the entropy reaches its maximum of (k_B ln 2) at this time. Similarly, the system energy decreases and the bath energy increases by the corresponding amount.

There are, however, also marked differences to the Lindblad model. First of all, the decay is nonexponential, with a slope $dP_1/dt = 0$ at $t = 0$, which is a clear signature of nonmarkovian behavior.[38] Second, at times longer than 500 fs, when $P_1 = \rho_{11} = 0$ and $P_0 = \rho_{00} = 1$, the excited state population rises again, reaching $\rho_{11} = 1$ after $t = 1000$ fs. In fact, an oscillatory behavior is observed with a period of ∼1000 fs. As a further difference to the Lindblad case we find that the reduced density matrix in the energy representation, when calculated from the full wave function $\Psi(t)$ according to eq 22, acquires small admixtures of the population-normalized off-diagonal elements (coherences) with time, which show also an oscillatory behavior. Albeit very small in the present example (on the order of 10^{-4}), this is a clear signature of population-coherence transfer which is absent in Lindblad dynamics.

For the resonant bath model the oscillations observed in Figure 2a are dominated by the coupling of the system to a single bath oscillator, which is resonant with the $|1\rangle \rightarrow |0\rangle$ transition within the system. This is demonstrated in Figure 3a, where, for the populations of the $v = 0$ and $v = 1$ states, the full bath MCTDH results are compared to MCTDH using a single

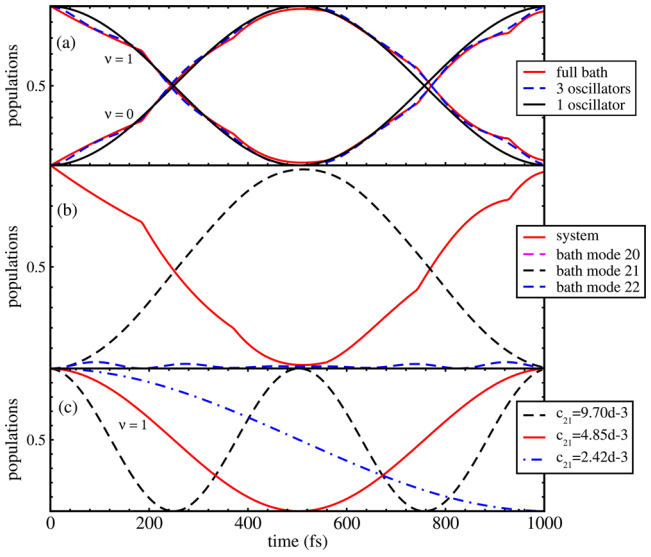

Figure 3. Time evolution of the subsystem and the bath populations for a resonant bath using MCTDH calculations, with an initial vibrational state of the subsystem v_0 = 1. (a) Populations of the subsystem taking into account the full bath, only one or three bath modes. (b) Population of the vibrational state v = 1 of the subsystem and the three dominant bath modes, 20, 21, and 22. (c) Population of the subsystem vibrational state v = 1 using three different subsystem−bath coupling strengths (in E_h/a_0^2 units) to resonant oscillator 21.

bath oscillator with $\omega_b = \omega_{1,0}$. With the single bath mode, the dynamics follows the same oscillatory behavior, with only small deviations from the full-bath case, which has a slightly more complicated structure. The smooth oscillations for the case of the single bath oscillator (the bath oscillator b = 21), can be interpreted as Rabi oscillations in a degenerate two-level system, between the initial state $|1_s0_b\rangle$ (one quantum in the system mode, none in the bath mode), and $|0_s1_b\rangle$ (no quantum in the system mode, one in the bath mode), coupled by a matrix element V. In this case, the exact solution of the time-dependent Schrödinger equation is analytically given as

$$P_{0_s1_b} = P_0 = \sin^2\left(\frac{|V|t}{\hbar}\right) \tag{26}$$

$$P_{1_s0_b} = P_1 = 1 - P_0 \tag{27}$$

with the corresponding oscillation period

$$T = \frac{\pi\hbar}{|V|} \tag{28}$$

The coupling term $V = \langle 1_s0_b|\hat{H}_{SB}|0_s1_b\rangle$ is

$$V = \langle 1|f(z)|0\rangle_z \sqrt{\frac{\hbar}{2m\omega_{1,0}}}\, c_b = \hbar\left(\frac{\gamma\Delta\omega}{2\pi}\right)^{1/2} \tag{29}$$

in the resonant single-oscillator case, where the approximate relation expressed in eq 29 holds under the double-harmonic approximation of above. In that case, $T \sim (2\pi^3/\gamma\Delta\omega)^{1/2}$. Using $\Delta\omega$ as specified above and γ^{-1} = 500 fs, gives $T \sim$ 960 fs, in good agreement with the observed period in the full bath case.

Adding more bath oscillators has only a small effect in the resonant-bath MCTDH model. This is also demonstrated in Figure 3a, which shows that with N = 3 bath oscillators (the resonant one, b = 21, and the two oscillators that are closest in energy to the resonant one, b = 22 and b = 20), the full-bath

dx.doi.org/10.1021/jp304466u | J. Phys. Chem. A 2012, 116, 11118−11127

model with $N = 40$ oscillators is already well reproduced. In Figure 3b then, the system mode evolution is accompanied by the full excitation of the resonant bath oscillator 21, whereas modes 20 and 22 are only very weakly populated, up to about 0.03 at most. Their particiaption cannot be entirely neglected, though and is responsible for the nonsmooth behavior of P_1 around $t \sim 180$ fs, $t \sim 370$ fs, ... At $t \sim 180$ fs, for example, the system oscillator loses energy only to the resonant bath oscillator 21, the other two modes restitute energy back to the system, and this is due to their different Rabi frequencies. The oscillation period of a nonresonant bath mode is roughly given by

$$T = \frac{2\pi\hbar}{\sqrt{4V^2 + \Delta^2}} \tag{30}$$

where V is its coupling to the Morse oscillator and Δ is its frequency detuning from resonance, i.e., $\Delta = \omega_b - \omega_{1,0}$. For instance, for bath modes 20 and 22, having the same detuning $|\Delta| = \Delta\omega$ and almost the same coupling V to the subsystem, their oscillation period is $T \sim 180$ fs.

Figure 3c shows the decay of the population of the subsystem interacting with only the single, resonant oscillator but with different coupling strengths, c_{21}. As the coupling between the subsystem and the bath gets stronger, the recurrence time gets smaller, and this is related to the Rabi frequency, which is inversely proportional to the coupling strength according to eqs 28 and 29. Equation 29 shows that the coupling matrix element, and thus the oscillation period, are dominated by the decay parameter, γ, and the bath frequency spacing, $\Delta\omega$.

Before closing this section, we want to clarify an important point regarding the recurrences observed in the time evolution of the subsystem. In true dissipative systems, where very large discrete baths are used, the "nominal" recurrence time is given by $T_{rec} = (2\pi\hbar/\Delta\omega)$, where $\Delta\omega$ is the smallest bath frequency spacing. It sets the time scale of an irreversible behavior; that is, energy cannot flow from the zero-temperature bath into the subsystem for times less than this recurrence time, also called Poincaré period. Thus, one may think that reversibility starts to occur exactly at this time. However, our study shows that for a small finite-size bath, the time at which recurrences in the subsystem observables start to occur can be longer, depending on the choice of the bath frequencies and the system−bath couplings. For instance, in our model of a resonant bath of 40 oscillators, with a frequency spacing $\Delta\omega = 179.5$ cm^{-1}, the bath nominal recurrence time is $T_{rec} = 186$ fs. However, recurrences in the subsystem start to occur at further times, namely at $T = 500$ fs for the subsystem $|1\rangle \rightarrow |0\rangle$ transition, as shown in Figure 3a. In fact, in this case, the subsystem interacts mainly with one resonant oscillator of the finite bath, and with a few oscillators close to resonance for a nonresonant bath, as can be seen in the next section. Consequently, a complete energy transfer from the subsystem to the bath is observed beyond the bath recurrence time, namely at half the Rabi oscillation period of the leading bath oscillator, given by eq 30. As such, the "subsystem recurrence time" depends on the detuning Δ, the coupling strength γ and also the bath frequency spacing $\Delta\omega$, through the coupling of the subsystem with the main bath oscillator. This can be seen, for example in Figure 3c where, for baths with the same frequency spacing $\Delta\omega = 179.5$ cm^{-1}, but different coupling strengths γ, we obtain different "subsystem recurrence times".

B. Nonresonant Bath. *B.1. Lindblad Model.* In this section, we present the results of vibrational energy transfer for the same system described above with the same parameters. The only difference is that the bath is slightly off-resonant with the Morse oscillator. This condition is encountered in many situations. For instance, if the bath is an extended molecular system, the frequencies of its vibrations may not necessarily match those of the subsystem it is interacting with. In our case, frequencies of the finite-dimensional bath are chosen to be equidistant as described above.

Figure 4 is equivalent to Figure 1b but for the nonresonant bath and demonstrates the Lindblad dynamics for the $v_0 = 1$ initial state, when coupled to the bath of 40 oscillators, treated by Fermi's Golden Rule. We observe that Lindblad calculations show the same behavior for population and information measures, whether the bath is resonant with the subsystem or not. In particular, a full energy transfer from the system to the bath is found. In fact, by the choice $\sigma = \Delta\omega$ for the Lorentzians in eq 17, we get approximately the same decay rate $\Gamma_{1\rightarrow 0} \sim \gamma^{-1} = 500$ fs as for the resonant Lindblad model. More precisely, we find $\Gamma_{1\rightarrow 0} = 520$ and 610 fs^{-1}, respectively, for the resonant and nonresonant model. The similarity of both cases is not a surprise, as the Lindblad formalism is tailored for true dissipative systems.

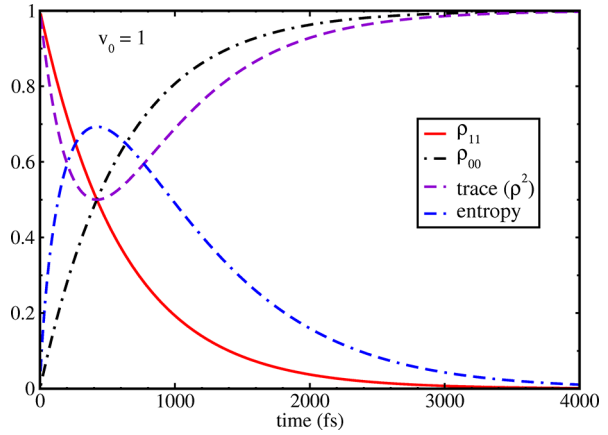

Figure 4. Time evolution of the subsystem populations, purity and entropy (in units of k_B), where the initial vibrational state of the subsystem is ($v_0 = 1$), using reduced density matrix calculations. Case of a nonresonant bath.

B.2. MCTDH Model. For the nonresonant case, exact dynamics calculations with MCTDH match neither the Lindblad results nor the exact dynamics for the resonant bath. This is demonstrated in Figure 5a, which is the same as Figure 2a for the nonresonant bath. It shows the populations of the states ($v = 0$, 1), the purity, and the entropy of the subsystem. We see qualitatively the same behavior as in the resonant case, namely a decay of the system excited state population, and recurrences. At short times (up to ∼180 fs), the nonresonant bath describes the same relaxation dynamics as with the resonant bath (notice that, up to the mentioned time, there is no difference between Figures 5a and 2a). However, at longer times, significant differences emerge. For instance, the subsystem does not lose all its excess energy before recurrences occur, and this is in contrast with what we observe with the resonant bath, and also in reduced density matrix calculations, showing a full energy transfer from the subsystem to the bath. It is seen that the population of system state $v = 1$ does not drop

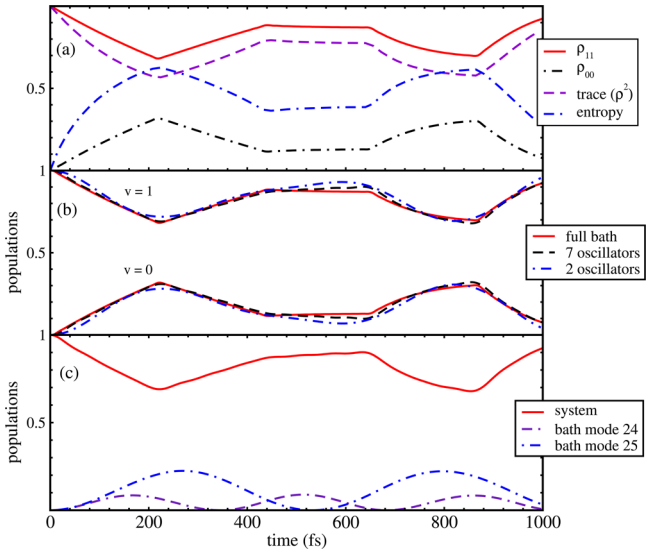

Figure 5. Vibrational relaxation of a Morse oscillator (v_0 = 1) interacting with a nonresonant bath using MCTDH calculations. (a) Time evolution of the subsystem populations, purity and entropy (in units of k_B). (b) Populations of the subsystem taking into account the full bath, only two or seven bath modes. (c) Population of the vibrational state v = 1 of the subsystem and the two dominant bath modes.

far below ρ_{11} = 0.7, and it is further observed that the oscillations are not smooth, with kinks and plateaus instead.

Figure 5b shows the populations of the subsystem vibrational states (v = 0, 1), using three different sets of calculations, taking into account (i) the full bath (i.e., 40 oscillators), (ii) two bath oscillators that are close to resonance (i.e., modes 24 and 25), and (iii) 7 bath oscillators with the closest frequencies to the frequency of the system (i.e., modes 22−28). The bath frequencies ω_{24} and ω_{25} are 3687 and 3841 cm^{-1}, respectively, detuned by Δ = −97 and +57 cm^{-1} from the fundamental system frequency of 3784 cm^{-1}. From Figure 5b we see that the two bath oscillators close to resonance dominate the dynamics, and with seven oscillators, we have almost achieved convergence.

To understand the irregular oscillations of the subsystem populations, especially the plateau region around 440−650 fs, we plot in Figure 5c the populations of state v = 1 of the subsystem and a bath with only the two most important modes (24 and 25). First, we should notice that the Rabi frequencies of the two modes are not the same, because of their different detunings with the system frequency. Their characteristic oscillation times, defined by eq 30, are $T_{24} \sim 345$ fs and $T_{25} \sim 535$ fs, respectively. As a result, it happens that one mode is populated whereas the other gives its energy back to the subsystem, and this gives almost no change in the population of the system state as shown by the plateau. With similar arguments, the kinks around t = 210 fs and at later times can be explained. Note further that bath oscillator 25, which has the smallest detuning of all bath oscillators, acquires more maximal population (∼0.2) than mode 24 or any other mode.

The fact that one, at most two, nonresonant bath oscillators determine the dynamics, explains also the incomplete population transfer from system to bath. For two states with coupling V and detuning Δ, the populations analogous to eq 26 are

$$P_{0_s 1_b} = P_0 = \frac{4V^2}{4V^2 + \Delta^2} \sin^2\left[\frac{\sqrt{4V^2 + \Delta^2}\, t}{2\hbar}\right] \tag{31}$$

Finite Δ accounts for a prefactor smaller than 1 and so for inclomplete population and energy transfer.

C. Lifetimes. In this section, we describe the dependence of lifetimes of the vibrational levels of the Morse oscillator on the vibrational quantum number. We then compare our exact results with the scaling law

$$\tau_v = \frac{\tau_1}{v} \tag{32}$$

as arising from eq 16.[24] Accordingly, lifetimes of vibrational levels are inversely proportional to their vibrational quantum number. Therefore, one usually calculates the lifetime of the first excited state and adopts this law for highly vibrational excited states. This law is derived from the assumptions that the vibrational mode of the subsystem is treated as harmonic and the system−bath coupling is linear in the system coordinates as outlined above. One can also compare the MCTDH results with another scaling law derived for a Morse oscillator linearly coupled to a bath of harmonic oscillators, which is given by[39]

$$\tau_v = \tau_1 \frac{(E_1 - E_0)}{(E_v - E_0)} \tag{33}$$

where E_n are the Morse oscillator vibrational energies. Again, this law predicts a monotonic decrease of the lifetimes with increasing vibrational quantum number. In our work, neither the vibrational mode is harmonic nor the system−bath coupling is linear in the system coordinate. So, it is interesting to investigate whether the scaling laws given by eqs 32 and 33 hold for our problem. Here, we do not analyze the nonresonant bath case, where some vibrational states merely lose a small amount of their populations before the appearance of recurrences, but only the resonant bath, for which the decay of the subsystem initial vibrational levels populations is complete. In other words, in the latter case, the recurrence time is large enough that a reasonable lifetime can be extracted from the first time window (i.e., before recurrences occur.) Also, because in the resonant model the population decay is not exponential, as a measure of lifetime, we take the time required for the population to drop to half of its initial value, i.e., the half-life time, $T_{1/2} = \ln 2 \cdot \tau$.

Figure 6a shows a comparison between MCTDH calculations and the above scaling laws (eq 32 and 33) for the half-life times of the vibrational levels of the Morse oscillator as a function of the vibrational quantum number. For fair comparison, the half-lifetimes have to be used in eqs 32 and 33 also. It is clear from the graph that the results given by both scaling laws are quite the same, so we will limit our discussion to a comparison between the results of MCDTH and the harmonic oscillator scaling law. The graph also shows that, for the low-lying vibrational levels (up to v_0 = 10), both the scaling laws and MCTDH show a decrease of the half-lifetimes with increasing quantum number of the initial vibrational state. In the graph, the values for v = 1 have been aligned, i.e., $T_{1/2}(v = 1, \text{MCTDH}) = T_{1/2}(v = 1, \text{ideal})$. However, even for these low energy levels, there is no quantitative agreement between the results given by the two curves. Apart from the increase in the anharmonicity of the Morse oscillator as the quantum number increases, the discrepancy between the scaling law and MCTDH in this vibrational range is mainly due to the form

dx.doi.org/10.1021/jp304466u | J. Phys. Chem. A 2012, 116, 11118−11127

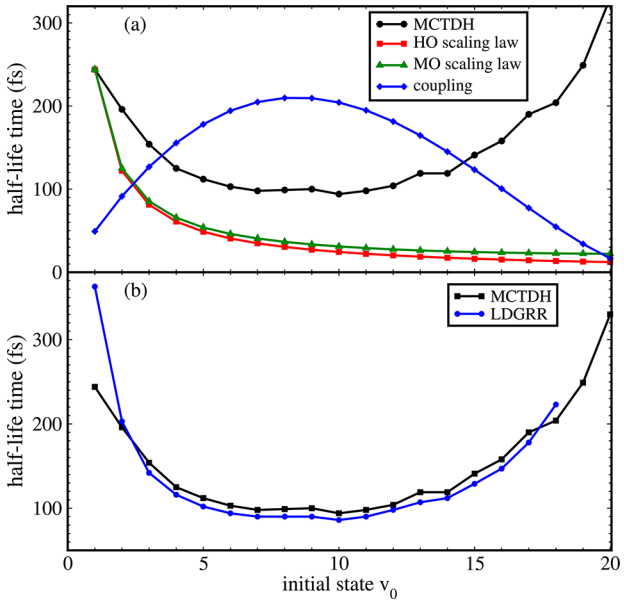

Figure 6. (a) Half-life times of the Morse oscillator vibrational levels obtained with MCTDH, and the harmonic and Morse oscillators scaling laws given by eqs 32 and 33. The matrix elements of the nonlinear interaction coupling ($\langle v|\exp(-\alpha z)|v-1\rangle$) are also shown (in arbitary units). (b) Comparison of MCTDH and Lindblad dynamics with golden rule rates (LDGRR) vibrational half-life times.

of the system−bath coupling being nonlinear. But the most striking result of our MCTDH calculations is the increase of the lifetimes of highly excited vibrations ($v_0 > 10$). Indeed, unlike the scaling law, which shows a continuous decrease of the lifetime when v_0 increases, exact calculations show a sharp rise in the lifetimes as we approach the dissociation limit.

The explanation for this behavior is also illustrated by Figure 6a, where we plot besides the half-life times, taken as the time required for the population to drop to half its initial value, also the coupling matrix elements between neighboring vibrational levels ($\langle v|\exp(-\alpha z)|v-1\rangle$), as functions of the initial vibrational quantum number. Although each initial vibrational state is coupled to all the lower vibrational levels, the couplings to the closest neighbors are dominant in the relaxation dynamics. Therefore, this coupling matrix element gives a good indication on the evolution of the transition rates as a function of the initial vibrational quantum number. The coupling matrix element is stronger for the vibrational levels in the middle of the spectrum of the subsystem; that is why their lifetimes are very low. However, it gets weaker for the low-lying states and those close to the dissociation limit. This is the reason for the sharp increase in the lifetimes of the highly excited states. For the scaling law, as it is derived assuming the vibrational levels being harmonic and the Hamiltonian interaction being linear in the subsystem coordinate, the squared coupling matrix elements of Figure 6a are then proportional to the quantum number v. Using these assumptions and Fermi's Golden Rule instead of the MCTDH propagation, leads then to the scaling law eq 32.

In Figure 6b, we compare the lifetimes of all the vibrational states obtained with MCTDH, and the Golden Rule/Lindblad formalism, which is mainly tailored for a true dissipative bath. The reduced dynamics results show the same behavior as MCTDH in the variation of the half-life times as a function of v. Thus, we draw an important conclusion on the surprising v dependence of the vibrational lifetimes: Although our MCTDH calculations deal with a finite-size bath, this behavior also holds for true dissipative environments. In fact, an exponential fitting of the short time vibrational population dynamics shows qualitatively the same behavior, i.e., a sharp increase of the lifetimes of the highly excited vibrational states. Therefore, we predict nonmonotonic behavior of lifetimes for adsorbate−surface vibrations with the level of vibrational excitation.

In passing we note that we have also investigated isotopic effects in the vibrational relaxation of the Morse oscillator by replacing OH by OD, coupled to a resonant 40-oscillator bath. Not surprisingly, on both the Lindblad/Golden Rule and MCTDH levels of theory, a behavior analogous to the one demonstrated in Figure 6 was found.

V. CONCLUSIONS

In this work, we have studied the vibrational relaxation of a Morse oscillator interacting nonlinearly with a finite size bath of harmonic oscillators at zero temperature with the help of two different approaches: exact dynamics (within the selected model) with MCTDH and reduced dynamics using the Lindblad formalism of reduced density matrix theory with rates obtained from Fermi's Golden Rule. We have investigated the dynamics of the process for all the vibrational states up to the dissociation limit, where we considered resonant and nonresonant baths. In the case of a resonant bath, for short times up to half the Rabi oscillation time dictated by the coupling to a resonant bath oscillator, reduced dynamics results agree reasonably well with exact dynamics results obtained with MCTDH. However, at longer times, Lindblad results fail to reproduce the recurrences in the time evolution of the subsystem observables as predicted by exact results. This is due to the markovian approximation introduced in the reduced density matrix formalism, a method tailored to describe truly dissipative dynamics, and as such, it does not take into account size effects of the environment.

For the subsystem $|1\rangle \rightarrow |0\rangle$ transition, with MCTDH calculations, we find that the single, resonant bath oscillator clearly dominates the dynamics, in agreement with general expectations (which are usually based on perturbative arguments). This situation may occur for instance in the case of a molecule in a solvent cage. Whenever the subsystem couples resonantly and weakly to one cage mode, the dynamics will essentially be trapped in a two-dimensional reduced space for all times.

In the nonresonant case, energy transfer from the system to the bath is incomplete and dominated by a few bath oscillators with the smallest detuning from the subsystem frequency. This means that, in the latter, the bath frequencies are poorly sampled to describe true dissipative dynamics. For such situations, a better frequency sampling of a bath, with a given number of modes, would be given by the eigenfrequencies of a chain with N-effective modes as suggested recently.[40]

On both the Lindblad/Golden Rule and MCTDH levels of theory, the time required for initial energy transfer from system to bath up to a "half-life time", decreases first with initial vibrational quantum number of the Morse oscillator and then increases again due to the effects of system anharmonicity and nonlinearity of the system−bath coupling in the system mode. This nonmonotonic lifetime behavior can be expected for all systems with large anharmonicities in system and coupling, notably for atoms or molecules at surfaces.

The next step of this study is toward the inclusion of larger baths to be able to describe true dissipative systems. This is clearly unfeasible with standard MCTDH due to its exponential scale limitation. However, new approximating schemes derived from the MCTDH formalism, such as *Gaussian* MCTDH (G-MCTDH)[25] or the *local coherent state approximation* (LCSA)[30] have been developed to tackle problems involving baths with a huge number of vibrational modes. In this thermodynamic limit the transition from discretized system−bath dynamics via the time-dependent Schrödinger equation to incoherent, dissipative dynamics via a reduced density operator formalism should become visible. The "exact" dynamics can always serve as a benchmark to test long-standing approximations of the reduced description, such as bath approximation, perturbation theory, Markov approximation, and secular approximation.[15] Other extensions of this work are to consider the temperature effects on the vibrational relaxation,[22] as well as the inclusion of the interaction with a laser field.[5,6] Finally, the modeling of concrete systems with more realistic bath and coupling models, can be a worthwhile task.

AUTHOR INFORMATION

Notes

The authors declare no competing financial interest.

ACKNOWLEDGMENTS

This paper is dedicated to Jörn Manz, a pioneer in time-dependent quantum molecular dynamics, on occasion of his 65th birthday. F.B. acknowledges the financial support of this work by the Alexander von Humboldt Foundation through a Humboldt research fellowship.

REFERENCES

(1) Nitzan, A. *Chemical Dynamics in Condensed Phases*; Oxford University Press: Oxford, U.K., 2006.
(2) May, V.; Kühn, O. *Charge and Energy Transfer Dynamics in Molecular Systems*; Wiley-VCH: Berlin, 2004.
(3) Feringa, B. L. *Molecular Switches*; Wiley-VCH: Weinheim, Germany, 2001.
(4) Manz, J.; Wöste, L. *Femtosecond Chemistry*; Verlag Chemie, Weinheim, Germany, 2001.
(5) Saalfrank, P. *Chem. Rev.* **2006**, *106*, 4116.
(6) Saalfrank, P.; Nest, M.; Andrianov, I.; Klamroth, T.; Kröner, D.; Beyvers, S. *J. Phys.: Condens. Matter* **2008**, *18*, 1425.
(7) Weiss, U. *Quantum Dissipative Systems*; World Scientific: Singapore, 2008.
(8) Breuer, H.-P.; Petruccione, F. *The Theory of Open Quantum Systems*; Oxford University Press: Oxford, U.K., 2002.
(9) Nest, M.; Meyer, H.-D. *J. Chem. Phys.* **2003**, *119*, 24.
(10) Burghardt, I.; Nest, M.; Worth, G. A. *J. Chem. Phys.* **2003**, *119*, 5364.
(11) Elran, Y.; Brumer, P. *J. Chem. Phys.* **2004**, *121*, 2673.
(12) Goletz, C.-M.; Grossmann, F. *J. Chem. Phys.* **2009**, *130*, 244107.
(13) Barnett, S. *Quantum Information*; Oxford University Press: Oxford, U.K., 2006.
(14) Brumer, P. W.; Shapiro, M. *Principles of the Quantum Control of Molecular Processes*; Wiley: New York, 2003.
(15) Blum, K. *Density Matrix Theory and Applications*; Plenum: New York, 1996.
(16) Redfield, A. *Adv. Magn. Reson.* **1965**, *1*, 1.
(17) Lindblad, G. *Commun. Math. Phys.* **1976**, *48*, 119.
(18) Gorini, V.; Kossakowski, A.; Sudarshan, E. C. G. *J. Math. Phys.* **1976**, *17*, 821.
(19) Breuer, H.-P. *Phys. Rev. A* **2007**, *75*, 022103.
(20) Meyer, H.-D.; Manthe, U.; Cederbaum, L. S. *Chem. Phys. Lett.* **1990**, *165*, 73. Manthe, U.; Meyer, H.-D.; Cederbaum, L. S. *J. Chem. Phys.* **1992**, *97*, 3199.
(21) Beck, M. H.; Jäckle, A.; Worth, G. A; Meyer, H.-D. *Phys. Rep.* **2000**, *324*, 1.
(22) Lüder, F.; Nest, M.; Saalfrank, P. *Theor. Chem. Acc.* **2010**, *127*, 183.
(23) Andrianov, I.; Saalfrank, P. *Chem. Phys. Lett.* **2006**, *433*, 91.
(24) Andrianov, I.; Saalfrank, P. *J. Chem. Phys.* **2006**, *124*, 034710.
(25) Burghardt, I.; Meyer, H.-D.; Cederbaum, L. S. *J. Chem. Phys.* **1999**, *111*, 2927.
(26) Wang, H.; Thoss, M. *J. Chem. Phys.* **2003**, *119*, 1289.
(27) Manthe, U. *J. Chem. Phys.* **2008**, *128*, 164116.
(28) Zhang, D. H.; Bao, W.; Yang, M.; Lee, S.-Y. *J. Chem. Phys.* **2005**, *122*, 091101.
(29) López-López, S.; Nest, M. *J. Chem. Phys.* **2010**, *132*, 104103.
(30) Martinazzo, R.; Nest, M.; Saalfrank, P.; Tantardini, G. F. *J. Chem. Phys.* **2006**, *125*, 194102.
(31) López-López, S.; Nest, M.; Martinazzo, R. *J. Chem. Phys.* **2011**, *134*, 014102.
(32) Paramonov, G. K.; Saalfrank, P. *Phys. Rev. A* **2009**, *79*, 013415.
(33) Light, J. C.; Hamilton, I. P.; Vill, J. V. *J. Chem. Phys.* **1985**, *82*, 1400.
(34) Colbert, D. T.; Miller, W. H. *J. Chem. Phys.* **1992**, *96*, 1982.
(35) http://www.pci.uni-heidelberg.de/cms/mctdh.html.
(36) Berman, M.; Kosloff, R.; Tal-Ezer, H. *J. Phys. A Math. Gen.* **1992**, *25*, 1283.
(37) Scheurer, Ch.; Saalfrank, P. *J. Chem. Phys.* **1996**, *104*, 2869.
(38) Paramonov, G. K.; Beyvers, S.; Andrianov, I.; Saalfrank, P. *Phys. Rev. B* **2007**, *75*, 045405.
(39) Nest, M.; Saalfrank, P. *Chem. Phys.* **2001**, *268*, 65.
(40) Martinazzo, R.; Hughes, K. H.; Burghardt, I. *Phys. Rev. E* **2011**, *84*, 030102(R).